

Hybrid Channel Model for Low Terahertz Links in a Data Center

JOHANNES M. ECKHARDT¹ (Member, IEEE), TOBIAS DOEKER¹ (Graduate Student Member, IEEE),
AND THOMAS KÜRNER¹ (Fellow, IEEE)

Institute for Communications Technology, Technische Universität Braunschweig, 38106 Braunschweig, Germany

CORRESPONDING AUTHOR: J. M. ECKHARDT (e-mail: j.eckhardt@tu-braunschweig.de)

This work was supported in part by the Federal Ministry of Education and Research of Germany in the program of "Souverän. Digital. Vernetzt." Joint Project 6G-RIC under Grant 16KISK031; in part by the Horizon 2020, the European Union's Framework Programme for Research and Innovation (TERAPOD) under Grant 761579; and in part by the Open Access Publication Funds of Technische Universität Braunschweig. This paper is part of the dissertation J. M. Eckhardt, "THz Communications in a Data Center: Channel Measurements, Modeling and Physical Layer Analysis," Düren, Germany: Shaker Verlag, 2024, [DOI: 10.24355/dbbs.084-202405061045-0].

ABSTRACT The aim of channel models is the effective prediction of wireless channels in application-specific environments in order to successfully design wireless communication systems. For THz communications, deterministic ray-optical channel predictions are very common. This paper shows inherent limitations of ray-tracing based models due to the accuracy of three-dimensional models of the environment in the context of THz communications and presents a new hybrid channel model approach that combines ray-optical channel predictions with an analytic path gain model extracted from measurements. The model is applied for switchable, point-to-point, wireless inter-rack links at THz frequencies in a data center that make the data center network reconfigurable at runtime. The channel parameters derived by the novel hybrid approach show promising results compared with channel parameters extracted from conducted reference measurements with an overall path gain error below 5 dB for residual multipath components.

INDEX TERMS THz, channel, channel model, data center, top-of-rack, multipath propagation, delay spread.

I. INTRODUCTION

TERAHERTZ (THz) communication is crucial for adding wireless connections in evolving data centers [1], transitioning from storage-centric to complex, computation-intensive tasks [2]. This evolution demands systems with ultra-low latency, high reliability, and scalable, flexible designs [3]. Current data center networks face limitations due to sporadic high-traffic bursts on underutilized links, which degrade service quality [4].

Wireless links, especially when combined with beam steering, significantly enhance data center network flexibility, allowing for dynamic reconfiguration [5]. Unlike traditional networks, which are costly and time-consuming to modify, wireless connections eliminate the constraints of physical cabling. This enables a software-defined network controller to adapt the network topology dynamically to meet changing demands and traffic patterns. Moreover, direct node-to-node

communication, bypassing aggregate and core switches, improves latency [6].

THz communications offer data rates comparable to those achieved through fiber optics transmission. In this context, the radio channel is fundamental in the development of THz communication systems, as it influences both system design and parameter selection. Therefore, a thorough understanding of the channel and proper modeling techniques are crucial for enabling this technology.

This paper presents a new hybrid channel modeling approach for THz communications that is applied to the data center use case. Based on an extensive measurement campaign [7], an analytic path loss approximation is derived that is combined with ray-optical channel predictions resulting in an application- and site-specific channel model. The contribution of the paper is fourfold:

- The paper examines the necessary level of detail of three-dimensional (3D) models used for ray-optical channel predictions at THz frequencies from a theoretic point of view. It shows that a deviation of 100 μm may have an impact on the reflection coefficient of optically thin media of more than 10 dB.
- A comparison of ray-optical channel predictions representing the current state of the art of THz channel modeling and double-directional channel measurements in a data center [7] evaluate the high accuracy in terms of angles and delay and shows the shortage in the prediction of the channel gain. More than 2/3 of relevant multipath components (MPCs) are identified in the simulation with a temporal and spatial accuracy below 5.7 ns and 4.2°, respectively.
- To compensate weaknesses in path gain modeling, a new channel model approach for THz channels is presented that combines ray-optical channel predictions with an analytical path gain model extracted from measurements reducing the overall path gain error below 5 dB.
- The hybrid channel model is applied to inter-rack links in a data center and the resulting channel parameters are validated against reference measurements providing satisfactory channel parameter characteristics that can be applied to higher layer simulations as well as system and protocol design.

The rest of the paper is structured as follows. Section II outlines different channel model approaches and gives a detailed overview of the state of the art and its shortcomings. Section III presents aspects on 3D models for deterministic ray-optical channel predictions and shows inherent limitations of this modeling approach in the context of THz communications. In Section IV, ray-optical channel predictions are conducted for and compared with the double-directional channel measurements in a data center scenario. Then, a novel hybrid channel model for wireless THz links in a data center is presented and validated in Section V. Finally, Section VI concludes the paper.

II. STATE OF THE ART OF THZ CHANNEL MODELS FOR DATA CENTERS

Channel measurements are time-consuming and cumbersome [8]. Sometimes the desired measurement is challenging or even not feasible. Therefore, models are developed that are a reproduction of the reality such that they incorporate important characteristics and attributes in the context of the application of interest. Since the reality is often very complex, a model might also serve as a simplification. Therefore, it is necessary to investigate how to effectively model THz channels in data centers in order to enable the development of THz communication systems. This section presents common channel model approaches and a detailed state of the art of channel models for THz communication in a data center.

A. MODELING APPROACHES FOR LOW THZ CHANNELS

Typically, models in the context of wireless channels have a certain validity range that is often limited. On the other hand, they might interpolate or predict new scenarios that have yet to be measured.

Regarding wireless channels, different modeling approaches exist. In the vehicular community, it is popular to classify channel models into geometry-based deterministic models, non-geometrical stochastic models, and geometry-based stochastic models [9]. Following this classification, this part briefly presents the idea of analytic, deterministic, and stochastic channel modeling approaches that can be applied for channels at THz frequencies.

1) ANALYTIC APPROACH

An analytic model describes the quantity of interest through a mathematical function. This might be a theoretically derived equation or a parameterized empirical expression. In the latter case, the coefficients are often fitted by minimizing cost function that is often the root mean squared error of the fit with regard to the measurements.

A popular example is the *A-B*-path loss model

$$L_{A-B,\text{dB}}(d) = A + B \cdot 10 \log_{10} \left(\frac{d}{d_{\text{ref}}} \right) + \epsilon, \quad (1)$$

with reference path loss A at reference distance d_{ref} , path loss exponent B and additive white Gaussian noise (AWGN) ϵ . It models the path loss as a function of the distance between transmitter (TX) and receiver (RX), d . Other channel parameters than the channel gain can be modeled in an analytic way as well [10].

The analytic approach is applied in THz communications among others to model the gain of individual MPCs such as *under-vehicle propagation* and *side reflection* in a vehicular setup in [11]. Also, the approach is adopted for *reflections at the seats* in an aircraft cabin that is based on geometrical considerations [12].

2) DETERMINISTIC APPROACH

A deterministic model includes all individual basic mechanisms that contribute to the modeled quantities in a determined and significant way. In doing so, the model combines the independent aspects and their interplay leads to a realistic characterization of the modeled quantity.

A prominent representative of deterministic model approaches are ray-optical channel prediction, also known as ray tracing. The ray tracing algorithms searches for paths, that retrace the propagation of waves motivated by the basic propagation mechanisms reflection, transmission, diffraction and scattering, in a geometrical model of the environment.

The higher the carrier frequency of the communication signal the better the wave can be described as a ray. Hence, the nature of THz propagation in complex environments favors ray-optical channel predictions [13]. The small wavelength leads to the fact that small objects already have an impact on the wave propagation. When represented in the

TABLE 1. Channel modeling approaches for low THz communications.

Type of model	Advantages	Drawbacks
Analytic approach	handy, easy to apply	limited complexity, dependency on few variables
Deterministic approach	precise if environment is well modeled	complex to implement
Stochastic approach	universal application	abstraction limits precision
Hybrid approach	combines advantages from different models	elaborate implementation

geometrical model, the ray tracing algorithm takes them into account in the path finding. In contrast to full-wave simulation tools, ray-optical channel predictions can handle large environments like lecture halls, industrial factories, data centers, and even outdoor environments.

3) STOCHASTIC APPROACH

Stochastic channel models represent a certain abstraction of a specific scenario to cover the wireless channel as a whole. On the basis of a data set originating either from measurements or other simulations techniques, probability density functions are fitted for the individual components of the system description, i.e., the impulse response [14].

A common approach is a combination of different channel model types. Based on a limited set of measurements, a ray tracing tool is calibrated that creates many realistic channel realizations in the scenario under investigation. The set of simulated channels is then again the basis for a stochastic channel model [15]. In this way, the information on the channel is made available to the community and applicable for link- and system level simulations in a general way.

B. RELATED WORK ON THZ CHANNELS IN DATA CENTERS

To effectively construct a new communication system operating at THz frequencies, in-depth study and accurate modeling of the radio channel are imperative. This step is necessary to tailor the physical layer and higher-layer protocols accordingly. Therefore, application- and site-specific channel models that incorporate propagation in complex environments, reflect multipath propagation, as well as the geometry and materials involved, are needed [8].

Han et al. provide in [16] a comprehensive survey on models for applications at THz frequencies. The following overview will be limited to channel models related to wireless links in data centers.

A first simulation-based model presented by Mollahasani and Onur in [17] in 2016 explores the impact of water vapor absorption using a free-space propagation model for frequencies up to 2 THz but lacks aspects on multipath propagation, temporal and spatial characteristics or any other environment-dependent aspects.

In [18], a more detailed simulation-based approach is outlined by Peng et al. in 2015 and adopted in 2016 by Fricke in [19] that develop a stochastic channel model derived from ray-tracing simulations within an idealized data center model

TABLE 2. Related work for low THz channel models in a data center.

Reference	Type	Description	Drawbacks
<i>Mollahasani et al.</i> [17]	analytic	channel model considering water vapor absorption	no multipath propagation considered
<i>Peng et al.</i> [18]	stochastic	broadband spatial model based on ray-tracing	purely simulation-based
<i>Fricke et al.</i> [19]	stochastic	broadband spatial model based on ray-tracing	purely simulation-based
<i>Cheng et al.</i> [20]	analytic, stochastic	gain and delay distributions	measurements in basic laboratory mock-up environment
<i>Cheng et al.</i> [21]	stochastic, geometrical	inter-rack model for OLoS links at medium height	limited link setups
<i>Cheng et al.</i> [22]	stochastic	inter-rack model at medium height	limited link setups
<i>Song et al.</i> [23]	analytic, stochastic	path gain model, examination of clusters	no temporal or spatial model
ITU [24]	analytic	path gain model	no temporal or spatial model

and offer simulated transfer functions of the radio channel in the frequency range of 252 GHz to 325 GHz. Unfortunately, the data set is purely simulations-based and no verification is performed.

A first measurement-based model was presented by Cheng et al. in [20] in 2019 that briefly summarizes the path loss and delay dispersion of a virtual multiple-input multiple-output (MIMO) measurement in a simplified mock-up scenario. Here, the setup located in an office room can hardly capture the environmentally features of a data center. The same authors describe the DOPPLER power spectrum of the narrow-band channel caused by vibrating cables due to the cooling airflow in a rack by a statistical two-ring model in [21]. Again, the setup is limited to a special use case of a link at medium height in an obstructed-line-of-sight (OLoS) scenario that does not capture spatial and temporal characteristics of the propagation channel due to multipath propagation.

The latest modeling approach for wireless links at 300 GHz was presented by Cheng et al. in [22] analyzing the multipath propagation for an inter-rack link at medium height. The proposed cluster-based model for the power delay profile (PDP) is based on the modified SALEH-VALENZUELA model and is derived from measurements for a single and fixed distance using optical lenses. This promising investigation discusses setups at medium height but omits top-of-rack links that are highly relevant for the data center use case.

Also in [23], Song et al. classify the multipath components into clusters. However, the methodology, the number of MPCs per cluster and the cluster specifics remain unclear. It is therefore incomplete to be used for the description of multipath propagation at THz frequencies in data centers.

Lastly, an *A-B*-path loss model with a power loss coefficient of 2.02 at 300 GHz is given in [24] by the International Telecommunication Union (ITU) without providing spatial or temporal information on the channel.

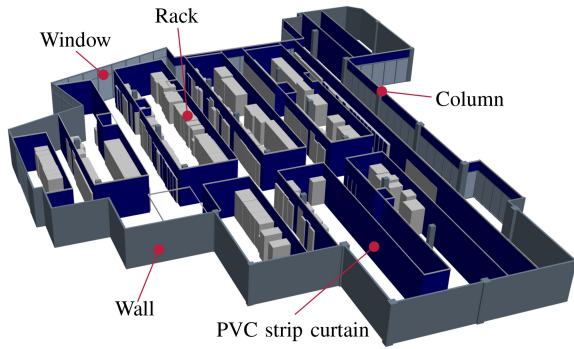


FIGURE 1. 3D model of the Dell EMC Research Data Center.

In conclusion, the literature review summarized in Table 2 shows that there are only two limited models that analyze multipath propagation in a data center, each focusing on a specific link type. Consequently, there is a shortage of geometrical channel models touching upon various link types under different propagation conditions that are suitable for the development of prospective THz communication systems in a data center.

C. PURSUED APPROACH

With regard to the presented modeling approaches, the deterministic model via ray-optical channel predictions represents a state-of-the-art and promising approach for realistic channel modeling at low THz frequencies in complex environments [16]. Also, the data center environment is too complex to model the channel exclusively with analytic and empirical equations. Moreover, the data set created by the measurements [25] is too small to create a reliable and significant stochastic model. Surprisingly, no validated ray-tracing simulations are reported in a data center up to now. However, ray-optical channel predictions incorporate the impact of the complex environment, leading to meaningful channel realizations in the context of wireless links in a specific data center if detailed information on the environment is available so that a 3D model can be built. Therefore, the approach followed in this paper uses ray-optical channel predictions as a basis for channel modeling and compensates limitations of ray-tracing with respect to the path gain prediction by an analytic path loss model.

III. DETERMINISTIC MODELING AT THz FREQUENCIES

A necessary component of a ray-optical channel prediction is a 3D model of the environment where the communication system under investigation is applied. This section discusses relevant aspects of 3D models, the role of material parameters and resulting limitations with regard to ray-optical channel predictions at THz frequencies.

A. CREATION OF THE 3D MODEL

To create a 3D model, the Dell EMC Research Data Center, Cork, Ireland where an extensive measurement campaign was conducted is documented in detail and technical drawings

of the various rack types, the polyvinyl chloride (PVC) strip curtains, the window facades, the columns, the room dimensions, and the positions of all items are made in parallel to the measurements.

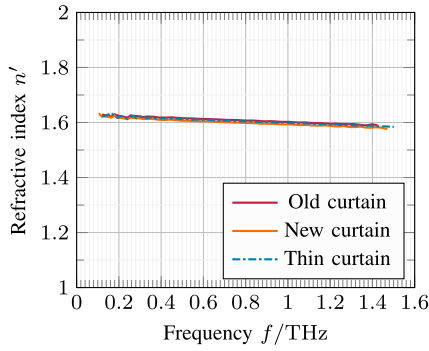
The 3D model is then created based on a modular approach. Generic and parametrized objects of each item type are defined in a local coordinate system on the basis of surfaces. Each surface is defined by a position vector, two direction vectors that define the plane in which the surface lies, and a tuple giving the vertices of the surface with respect to the direction vectors. The complete model is finally built by lists that contain the concrete items present in the data center. The position of each item is defined by a position vector in the global coordinate system of the model. It can be freely scaled by a given width, a height, and a depth and oriented by two vectors that define the relation between the local coordinate system and the global coordinate system.

In order to account for the impact of different materials in the environment, a material parameter is assigned to each surface that contains the complex permittivity, the thickness, the roughness, and the correlation length [26]. The racks are mainly made out of powder-coated metal, but some types have a plastic front that is modeled as high-density polyethylene (HDPE). The floor is given by glass fiber-reinforced laminate, whereas the walls, the columns, and the ceiling are assumed as concrete. The door is made out of laminated beech wood and the windows out of glass with a metal frame. The strip curtains consists of a metal rail and a PVC curtain. The geometrical model of the Dell EMC Research Data Center is shown in Fig. 1, where the floor and the ceiling are omitted for the sake of clearness. Concrete is depicted in dark gray, metal in light gray, PVC and HDPE in dark blue, glass in light blue, and wood in brown.

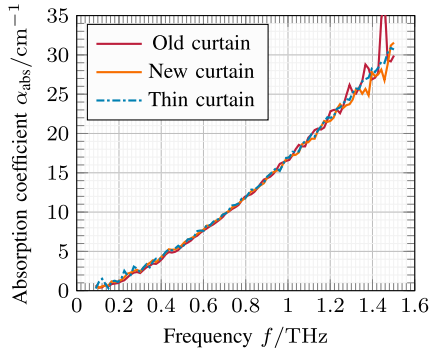
Materials parameters of building materials relevant for THz communications are reported among others in [26], [27], [28], [29], [30], [31] whereas metal can be approximated for relevant frequencies with relative permittivity $\epsilon_r = 1 + j10^7$ [32], [33].

A specific object of special importance in the data center under investigation represent the plastic curtains. Therefore, three material probes of the three different kinds of PVC strip curtains have been characterized by the National Physics Laboratory (NPL), Teddington, UK, in the framework of the European Project “Terahertz Based Ultra High Bandwidth Wireless Access Networks” (TERAPOD) [34]. The first sample is a piece of an older curtain that is partly covered with a kind of flour and less transparent compared to the second sample that is a brand-new transparent PVC strip curtain. Both types of curtains have a thickness of 3.70 mm. The third sample is also a brand-new piece of curtain that is thinner with a thickness of approximately 3.0 mm.

The measured refractive indices n' that are presented in Fig. 2(a) show only a marginal difference between the samples and decreases slightly from 1.62 at 100 GHz to 1.58 at 1.5 THz. The absorption coefficient α_{abs} increases from 0.5 cm^{-1} at 100 GHz to 30 cm^{-1} at 1.5 THz and is visualized



(a) Refractive index



(b) Absorption coefficient

FIGURE 2. Material parameters of the plastic curtains.

in Fig. 2(b). At the frequency of interest of 300 GHz the refractive index and the absorption coefficient of the old curtain sample yield 1.62 and 2.24 cm^{-1} , respectively. A more detailed description of the role of material parameters in 3D models can be found in [35].

B. DIELECTRIC BOUNDARY LAYER

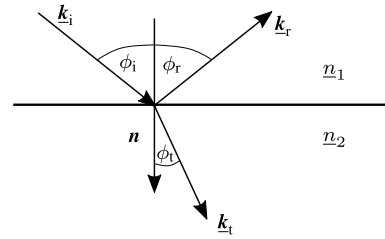
The environment of a wireless communication system is full of things and items that interact with the electromagnetic waves and manipulate the channel. When an incident wave hits a dielectric boundary layer reflection and diffraction takes place. Fig. 3(a) illustrates the interaction with the dielectric boundary layer where ϕ_i , ϕ_r , ϕ_t and \underline{k} denote the angle of incidence, the angle of reflection, the angle of transmission and the wave vector, respectively.

The complex FRESNEL transmission and reflection coefficients for transverse magnetic (TM) and transverse electric (TE) polarization are a good approach to model this interaction and specify the ratios of the incident electric field and the reflected or transmitted electric fields. They depend on the angle of incidence and are given by [36]

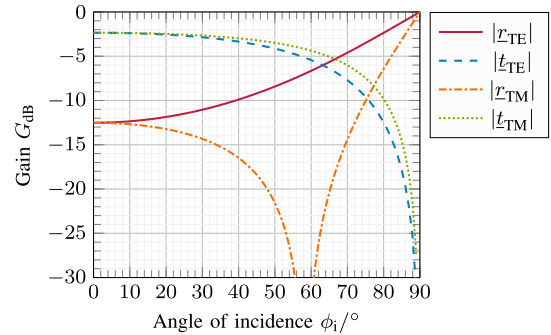
$$r_{\text{TE}} = \frac{\underline{Z}_2 \cos \phi_i - \underline{Z}_1 \cos \phi_t}{\underline{Z}_2 \cos \phi_i + \underline{Z}_1 \cos \phi_t} \quad (2)$$

$$t_{\text{TE}} = \frac{2\underline{Z}_2 \cos \phi_i}{\underline{Z}_2 \cos \phi_i + \underline{Z}_1 \cos \phi_t} \quad (3)$$

$$r_{\text{TM}} = \frac{\underline{Z}_2 \cos \phi_t - \underline{Z}_1 \cos \phi_i}{\underline{Z}_2 \cos \phi_t + \underline{Z}_1 \cos \phi_i} \quad (4)$$



(a) Schematic illustration based on BORNPrinciplesOptics60th2019



(b) FRESNEL coefficients

FIGURE 3. Reflection and transmission coefficients at a single dielectric boundary layer.

$$t_{\text{TM}} = \frac{2\underline{Z}_2 \cos \phi_i}{\underline{Z}_2 \cos \phi_t - \underline{Z}_1 \cos \phi_i}, \quad (5)$$

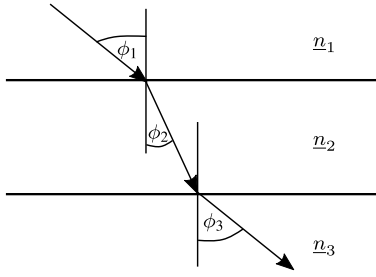
where r , t and \underline{Z} denote the reflection coefficient, the transmission coefficient and the wave impedance, respectively.

The examination of the FRESNEL coefficients of the presented plastic curtains that are visualized in Fig. 3(b) shows an absolute value of the reflection coefficient and the transmission coefficient of -12.5 dB and -2.3 dB for an incident angle $\phi_i = 0^\circ$, respectively. The BREWSTER angle – the angle at which the reflection coefficient for TM polarization yields $r_{\text{TM}} = 0$ – is given at 59° .

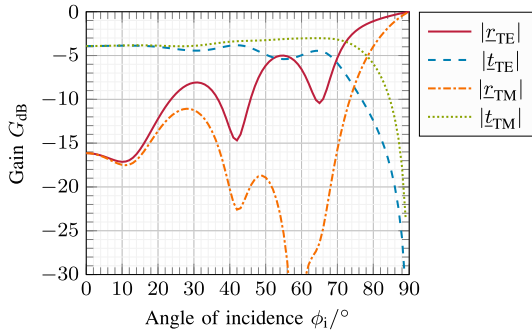
However, the path loss measured in the point-to-point (P2P) top-of-rack (ToR) setup for reflected links that is presented in [7] shows a high reflection loss of approximately 28 dB for an angle of incidence $\phi_i = 8^\circ$. Consequently, the FRESNEL coefficients do not seem appropriate to model the characteristics of the PVC strip curtains.

C. PROPAGATION IN A STRATIFIED MEDIUM

The deviation of the FRESNEL reflection coefficients and the measurement can be explained by the fact that the plastic curtains represent an optically thin medium so that also the second boundary interface – the backside of the curtain from PVC to air – has a significant impact on the transmission and reflection. Hence, there is a need for a more detailed model. A so-called stratified medium with multiple layers can be described by the transfer matrix method and the characteristic matrix of a stratified medium [37]. For a stratified medium



(a) Schematic illustration based on BORNPrinciplesOptics60th2019



(b) Reflection and transmission coefficients

FIGURE 4. Reflection and transmission coefficients of the stratified medium.

with three layers as illustrated in Fig. 4(a) and represented by the plastic curtain (air – PVC – air), the reflection and transmission coefficients can be written as

$$r_{\text{SF}} = \frac{r_{12} + r_{23} e^{2j\beta_{\text{SF}}}}{1 + r_{12}r_{23} e^{2j\beta_{\text{SF}}}} \quad (6)$$

$$t_{\text{SF}} = \frac{t_{12}t_{23} e^{2j\beta_{\text{SF}}}}{1 + r_{12}r_{23} e^{2j\beta_{\text{SF}}}}, \quad (7)$$

where r_{xx} and t_{xx} denote the FRESNEL reflection and transmission coefficients of the respective boundary layer and respective polarization. β_{SF} denotes a phase factor given by

$$\beta_{\text{SF}} = \frac{2\pi}{\lambda_0} \cdot n_2 h \cos \phi_2, \quad (8)$$

where λ_0 , h , n_2 , and ϕ_2 denote the wavelength in vacuum, the thickness of the second medium, the refractive index of the second medium and the angle in the second medium, respectively.

The reflection and transmission coefficients of the PVC curtain modeled as stratified medium with a thickness of 3.70 mm are shown in Fig. 4(b) for both, TE and TM polarization. The reflection coefficient of TE polarization is generally greater than the reflection coefficient of TM polarization but both polarizations show multiple minima at angles of incidence of 11°, 42° and 65°. The transmission loss is relatively low with values below 5 dB for angles smaller than 70°. Comparing the model with the measured reflection loss, the reflection coefficient of the stratified medium of –17 dB for an angle of incidence of 8° reduces

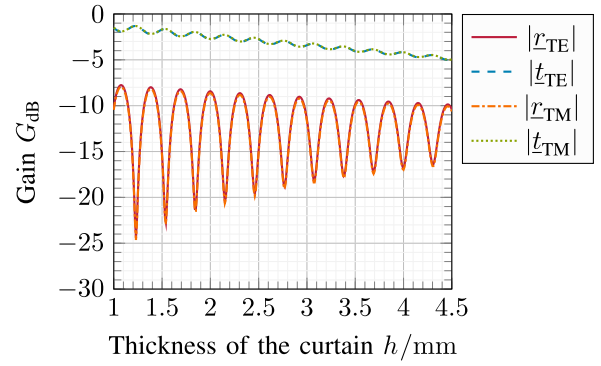


FIGURE 5. Reflection and transmission coefficients of the plastic curtain for $\phi_1 = 8^\circ$.

the deviation from the measurement by 4.5 dB. Other sources for the measurement inaccuracy might be a fragile antenna alignment and positioning or a slight twist of the curtain so that the specular reflection is not properly captured.

It is now of interest to estimate the robustness of the model with regard to the level of detail of the 3D model of the environment. The PVC strip curtain has mainly a thickness of 3.70 mm but at some points close to the edge the thickness reduces to 3.65 mm. Fig. 5 shows the dependency of the reflection and transmission coefficients on the thickness h of the intermediate layer for an angle of incidence of 8°. The transmission coefficients vary slightly in a wavelike manner by only 4 dB whereas the reflection coefficients vary between –7.8 dB and destructive interference of more than –25 dB. The minima and maxima are 0.15 mm apart and already a deviation of the thickness of only 0.1 mm causes a change of the reflection coefficient of 13.4 dB. Hence, the level of detail that is necessary to model the interaction with matter in a satisfactory manner with an accuracy of a few dB lies in the order of 100 μm . This result sets unrealizable requirements on the 3D model in complex environments with dimensions of multiple tens of meters. The effect of this finding on the channel model via ray-optical channel predictions is discussed in the following section.

IV. RAY-OPTICAL CHANNEL PREDICTIONS

In this section, deterministic channel modeling via ray-optical channel predictions with the Simulator for Mobile Networks (SiMoNe) is applied to wireless links in a data center and compared with channel measurements from [7].

A. FUNCTIONALITIES OF THE SIMULATION TOOL

SiMoNe [38] is a multi-level simulation suite that includes channel predictions [39], link level simulations [40] and system level simulations [41]. The channel prediction functionalities provide among others a channel predictor called *FemtoPred* that implements a ray tracing module and stochastic models like the OKUMURA-HATA model. Here, only the ray tracing module is applied for the

following investigations that are conducted with SiMoNe v2023.01 [38].

The *FemtoPred* requires information about the environment in form of a 3D model explained in Section III-A. The position of the TX and RX is set in the scenario definition. The ray tracing engine predicts the propagation channel in a two-step approach. First, the search for geometric paths between the TX and RX is done. The result of this step consists of rays characterized by an angle of departure (AoD), angle of arrival (AoA) and interactions points at the surfaces. In the second step, electromagnetic models are applied to predict the complex amplitude of the MPCs.

The ray search is conducted individually for each basic propagation mechanisms – direct path, reflection, scattering, and diffraction. Reflection is sometimes divided into specular reflection and non-specular reflection where the latter one corresponds to scattering. The direct path is calculated based on the positions of TX and RX and the potential transmission through surfaces is checked. Here, free-space path loss and if applicable the transfer matrix method for stratified media are applied to calculate the path loss and the transmission loss, respectively. Reflected paths are calculated based on the principle of image sources that mirror the TX at each surface in order to find a possible reflection point [42]. Depending on the selected order of reflection this procedure is repeated multiple times. The reflection coefficients at each interaction point are also determined by the transfer matrix method as described in Section III-C. In order to find scattered rays, the surfaces that have a line-of-sight (LoS) connection to TX and RX are basically divided into tiles with a certain tile size. If a LoS connection persists for the individual scatter tile, the ray via the tile is valid. The complex amplitude of the ray is modeled by the modified equivalent current approximation (MECA) [43].

Current limitations of the prediction tool affect the polarization since TE and TM components are averaged at each interaction point. Also, the literature suggests the application of KIRCHHOFF scattering and the modified FRESNEL reflection and transmission coefficients in the context of THz communications [44], [45].

B. SIMULATION SETUP AND CONDUCT

Within the created 3D model of the data center, the scenarios of the double-directional channel measurements from [7] are emulated and TX and RX are placed at the positions given in [25]. An isotropic antenna is assumed in order to simulate the propagation channel. A library of the material parameters listed in Table 3 is selected so that the corresponding parameters are assigned to the respective surfaces. In contrast to the common approach of calibration of the material parameters [46], [47], the original material parameters are unchanged in order to retain the physical relation in the simulation.

Reminding the propagation conditions, all medium height (MH) measurement positions and the ToR1 position are a LoS scenario whereas the ToR2 to ToR5 are OLoS scenarios.

TABLE 3. Material parameters applied in the simulation at 300 GHz.

Material	ϵ'_r	ϵ''_r	n'	$\alpha_{\text{abs}}/\text{cm}^{-1}$	Source
PVC plastic	2.62	0.058	1.62	2.24	measurement
HDPE plastic	2.34	0.0023	1.53	0.11	[26]
Glass fiber-reinforced laminate	4.58	0.21	2.14	7.15	[26]
Concrete / sand-lime brick	3.49	0.23	1.87	9.09	[26]
Glass	6.65	0.35	2.58	9.95	[26]
Laminated beech wood	2.10	0.12	1.45	6.3	[26]
Metal / aluminum	1	10^7	-	-	[32], [33]

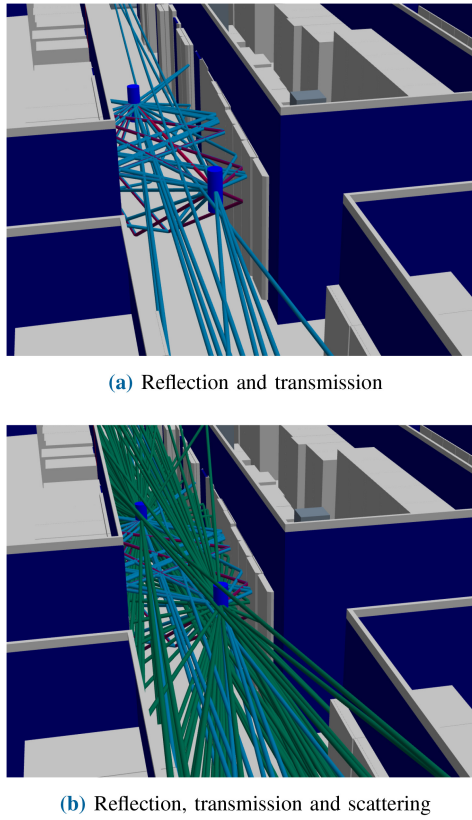
The simulation is configured in such a way that in MH scenarios reflections up to the third order are searched and transmissions up to the second order are allowed. In ToR scenarios, also reflections up to the third order are searched but transmissions up to the eighth order are allowed. For transmission, each interaction layer is counted so that one curtain represent already two interaction layers with its front and back side. Therefore, this configuration is justified by the environment that is more penetrable at ToR level with the PVC strip curtains compared to the metal racks at MH. Diffraction is not considered in the simulation since its impact is assumed to be negligible in the LoS and OLoS scenarios under investigation [48]. Since transmission is not supported in combination with scattering, scattered rays occur only in LoS scenarios. After a successful execution of the simulation flow, the MPCs can be exported and post-processed in MATLAB[®].

C. COMPARISON OF SIMULATIONS AND MEASUREMENTS

1) QUALITATIVE COMPARISON

The MPCs of the simulated propagation channels are compared to the measurement results presented in [7] in order to evaluate the quality of the simulation approach. Fig. 6 illustrates the simulation of the setup MH2. TX and RX are representatively depicted as dark blue cylinders. The direct path is plotted in red, reflected paths are plotted in light blue, and transmitted and reflected paths are plotted in violet. For the sake of visibility, Fig. 6(a) omits the scattered path that are additionally illustrated in green in Fig. 6(b).

First, the power angular profiles (PAPs) of the simulation and the measurement are compared. Fig. 7(c) shows the PAPs of MH2 that correspond to the setup in Fig. 6. The MPCs of the measurement are depicted with circles whereas the simulation is illustrated with crosses. The size and color of the markers is scaled to the respective channel gain. In Fig. 7(a) it is clearly visible that the strong MPCs of the measurement are covered by reflected MPCs. Three times, the simulation predicts a MPC where no MPC was measured. The scattered MPCs that are additionally shown in Fig. 7(b) mainly lie on a cross-shaped trajectory around the direct path and cover several measured MPCs. This cross-shaped trajectory is also observed in MH1, aircraft cabins [12] and high speed train wagons [49] that all have a corridor-like environment. Hence, scattering has an important contribution to the propagation


FIGURE 6. Visualization of the reflected and scattered rays of MH2.

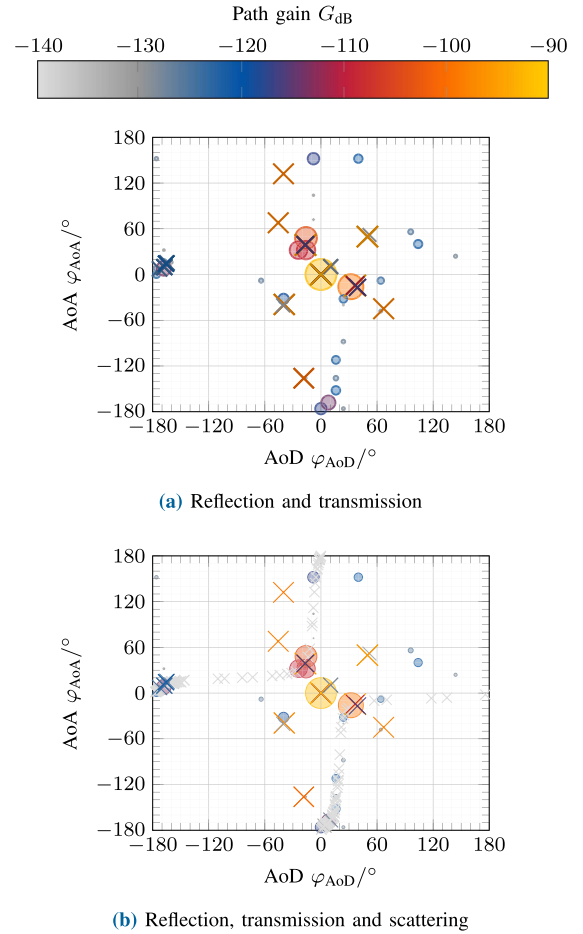
channel at THz frequencies also with regard to relevant THz applications. In conclusion, two measured and striking MPC were not predicted by the simulation.

The comparison of the PDPs gives insights about the temporal agreement of the simulation and the measurement. Two exemplary comparisons of MH2 and ToR1 are presented in Fig. 8. Fig. 8(a) presents the just discussed setup MH2. In all regions of measured MPCs also simulated MPCs are present. Inversely, the gap between 70 ns and 90 ns is clearly visible in the simulation and the measurement. However, the gain of the simulated MPCs differs significantly – for some MPCs up to 30 dB – from the measured path gain. The early MPCs up to a delay of 30 ns are overestimated and later MPCs that are mainly cause by scattering are underestimated. A similar characteristic is visible in the ToR1 setup presented in Fig. 8(b). Early paths are overestimated and a group of simulated paths around a delay of 38 ns are not measured.

2) QUANTITATIVE COMPARISON

In order to obtain a quantitative measure of the simulation accuracy a ray matching between the simulated and measured rays is performed and the mean absolute error (MAE) is calculated afterwards. The matching of the simulated and measured MPCs is conducted in three steps. First, every simulated MPC is assigned to the measured MPC for which the following error criterion is minimal,

$$E_{\text{RayMatch}} = \left(\frac{\tau_{\text{meas},l}}{\text{ns}} - \frac{\tau_{\text{sim},l}}{\text{ns}} \right)^2$$


FIGURE 7. Comparison of the PAPs of MH2.

$$\begin{aligned} & + \left(\frac{\varphi_{\text{TX,meas},l}}{\circ} - \frac{\varphi_{\text{TX,sim},l}}{\circ} \right)^2 \\ & + \left(\frac{\varphi_{\text{RX,meas},l}}{\circ} - \frac{\varphi_{\text{RX,sim},l}}{\circ} \right)^2. \end{aligned} \quad (9)$$

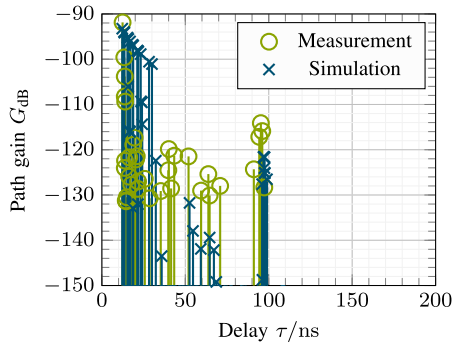
Here, only geometrical aspects of the MPCs are considered for the assignment and an error of 1 ns in the delay domain has the same impact as an error of 1° in the angular domain. Second, for every measured MPC the simulated MPC with the lowest error of the group of assigned, simulated MPCs is selected so that pairs of measured and simulated MPCs are created. Third, the criteria of acceptance

$$\Delta\tau_l = |\tau_{\text{meas},l} - \tau_{\text{sim},l}| < 10 \text{ ns} \quad (10)$$

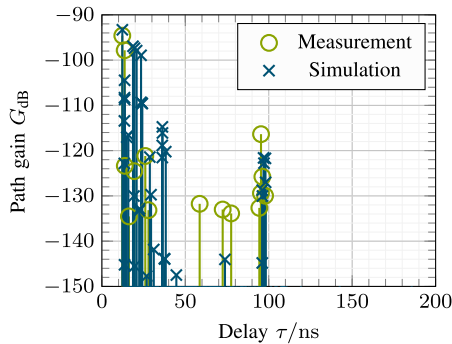
$$\Delta\varphi_{\text{TX},l} = |\varphi_{\text{TX,meas},l} - \varphi_{\text{TX,sim},l}| < 20^\circ \quad (11)$$

$$\Delta\varphi_{\text{RX},l} = |\varphi_{\text{RX,meas},l} - \varphi_{\text{RX,sim},l}| < 20^\circ \quad (12)$$

check that only MPCs with a reasonable mismatch belong together and are compared. Table 4 presents the ratios of the number of matched MPCs to the number of measured MPCs, denoted as R , broken down by a threshold that only takes into account the MPCs with an additional path loss below the respective threshold. In this ratio, the numerator represents the number of matched MPCs and the denominator represents the number of measured MPCs. Most scenarios show a very good match. However, MH4



(a) MH2 measurement



(b) ToR1 measurement

FIGURE 8. Comparison of the PDP of the double-directional propagation channel.

TABLE 4. Overview of matched MPCs for different thresholds.

Scenario	$R_{10\text{ dB}}$	$R_{20\text{ dB}}$	$R_{30\text{ dB}}$	R_{all}
MH1	2/2	3/4	11/25	38/114
MH2	2/2	5/5	12/15	27/36
MH4	2/3	6/8	8/38	29/189
ToR1	2/2	2/2	6/6	11/16
ToR2	1/1	2/3	2/5	5/17
ToR4	1/1	1/1	2/4	12/50

TABLE 5. MAE between simulated and measured MPCs.

Scenario	$E_{\text{MAE},\tau/\text{ns}}$	$E_{\text{MAE},\text{AoD}/^\circ}$	$E_{\text{MAE},\text{AoA}/^\circ}$
MH1	1.11	3.2	4.2
MH2	0.92	1.9	3.0
MH4	2.87	3.3	4.1
ToR1	1.17	3.1	2.4
ToR2	1.35	3.3	2.6
ToR4	5.69	4.2	3.5

demonstrates a lower 10 dB-ratio $R_{10\text{ dB}}$. Notably, MH4 is the scenario with the highest level of multipath propagation and its 20 dB-ratio $R_{20\text{ dB}}$ is still very acceptable.

Finally, the MAE is calculated for the delay, the AoD, and the AoA according to the following principle

$$E_{\text{MAE},\tau} = \frac{1}{L} \sum_{l=1}^L |\tau_{\text{RT},l} - \tau_{\text{meas},l}|, \quad (13)$$

where l and L denote the index of the matched MPC and the number of matched MPCs, respectively. Table 5 shows the individual MAEs for the different scenarios. The MAEs are well below the respective criterion of acceptance so that the criterion itself does not influence the MAE. The delay and angular information of the simulations matches well. In only two scenarios, the MAE of the delay is greater than 1.4 ns corresponding to a path length of 0.42 m. Also the MAE in the angular domain stays always below 4.2° that can already be explained by the raster scan pattern of the double-directional channel measurements with a step size of 8° .

3) CONCLUDING DISCUSSIONS

The accuracy of the simulated path gain is not satisfactory and critical for the design and simulation of novel THz applications. There are multiple reasons of different nature that lead to this fact.

First, the necessary level of detail of the 3D model is not achievable. As demonstrated in Section III, the accuracy lies in the order of $100\ \mu\text{m}$ for the thickness of the PVC strip curtains. The comparison shows that the geometrical dimensions of the 3D model are sufficient for the MPCs finding but the geometrical and material related aspects with an impact on the path gain are deficiently represented.

Second, the ray tracing algorithms considers single interaction points when calculating the reflection and transmission coefficients and neglects the illuminated area by the incident beam or wavefront. Here, the front door of certain rack models is fabricated with a powder-coated, perforated metal with a whole diameter in the order of 5 mm. A material characterization of the powder-coated metal will not be sufficient to adequately model the reflection and transmission properties of the metal sheet and would overestimate the reflection as visible in Fig. 8(a). Hence, it is challenging to characterize all materials in a complex environment with their permittivity, roughness and thickness in the necessary level of detail.

Consequently, in spite of the state-of-the-art implementations of propagation mechanisms like the transfer matrix method or KIRCHOFF scattering considering the roughness of the surfaces, an expedient channel model with a pure ray tracing approach based on the physical characteristics of the environment is hardly possible.

V. A HYBRID CHANNEL MODEL FOR LOW THZ LINKS IN A DATA CENTER

The following section presents a novel hybrid model approach that combines deterministic ray-optical channel predictions and analytical modeling. In the literature, state-of-the-art ray-tracing approaches perform a calibration of the material parameters of the 3D model in order to achieve a good match of the path gain between simulation and measurements [46], [47]. However, in this way, the model is decoupled from the physical interpretation of permittivity and the transfer to other setups in the same environment is still an open research question. The following hybrid model

for low THz links in a data center merges the accurate geometric predictions of ray-tracing with an analytically fitted description of the path gain.

A. MODEL DESCRIPTION

The model combines the benefits of two modeling approaches. More specifically, it takes advantage of the high precision of ray-optical channel predictions with respect to the geometric information that are demonstrated in Section IV and the experience gained with regard to the path gain distribution in the comparison of multiple scenarios for low THz communications [50]. First, the deterministic aspects are discussed followed by the empirical, analytic component related to the path gain.

1) DETERMINISTIC CHANNEL ASPECTS

The deterministic channel aspects base on the contributions of the ray-optical channel predictions. The literature and the previously described results show that path finding algorithms and the geometrical examination are well suited for modeling channels at THz frequencies. The level of detail for a specific scenario that is provided by deterministic models is mandatory for a reliable simulation and system design of prospective THz communication systems. The basis for this activity remains a 3D model of the environment with cm-scale precision. The scenario under investigation is configured and the ray-tracing simulation is conducted as previously described. The obtained MPCs are sorted with respect to their path gain resulting in the intermediate outcome that consists of the MPCs with amplitude A_l , delay τ_l , AoD $\varphi_{AoD,l}$, and AoA $\varphi_{AoA,l}$.

2) ANALYTICAL MODELING ASPECTS

The uniform analysis of 56 measurement positions in five different environments has shown an exponential decrease of the normalized gain of the MPCs in dB scale for all measurement positions [50]. Hence, the slope of the normalized path gains seems typical for application-related channels at THz frequencies and a collaborative modeling approach on the bases of the measured path gain can be determined and replace the erroneous path gain of the MPCs from the ray-tracing simulation. The function

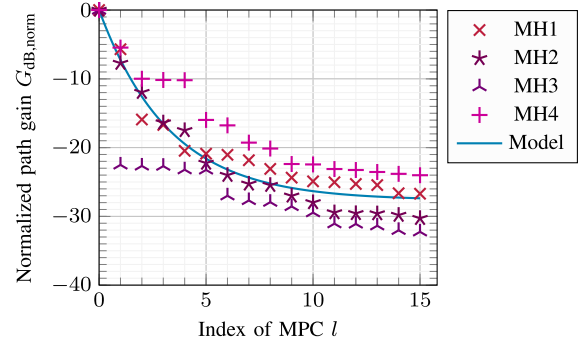
$$G_{dB, \text{norm}, l} = \alpha e^{-\beta l} - \alpha, \quad (14)$$

is proposed to model the normalized path gain as a function of the MPC index l where α and β are the coefficients that account for the minimum normalized path gain and the slope, respectively. As a reminder, the MPC index l numbers the MPCs sorted by their path gain.

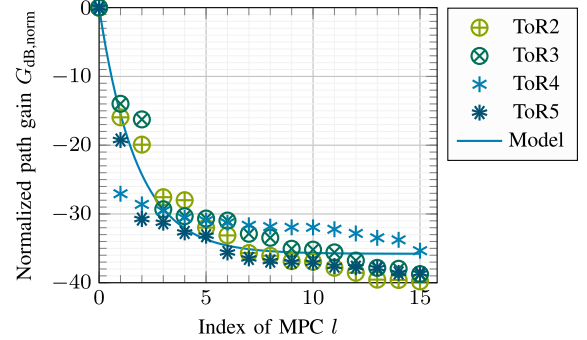
Depending on the environment and the LoS condition the curve progression of the normalized MPCs varies. Therefore, a classification as a function of the scenario and the LoS condition has to be taken into account and is fundamental for a meaningful model. For each class, an individual set of model coefficients α , β has to be determined.

TABLE 6. Model coefficients in a data center.

(a) Propagation channel			(b) Radio channel		
Scenario	α	β	Scenario	α	β
MH LoS	27.66	0.304	MH LoS	41.87	0.802
ToR LoS	39.41	0.306	ToR LoS	44.89	0.772
ToR OLoS	35.79	0.567	ToR OLoS	45.02	1.134



(a) MH LoS scenario



(b) ToR OLoS scenario

FIGURE 9. MPCs and approximation of the double-directional propagation channel.

The classification of wireless links in a data center is earlier presented in [7]. Based on the channel properties derived from double-directional measurements, the categories MH LoS, ToR LoS, and ToR OLoS for the propagation channel and the radio channel, respectively, are identified. The coefficients are selected such that the mean squared error is minimal considering the first 15 MPCs. If an MPC is below the threshold of 40 dB and hence not represented in the available data, the MPC is assumed with a normalized path gain of -45 dB in order to assure a fair weighting of the MPCs. Table 6 presents the model coefficients of the propagation channel and the model coefficients of the radio channel. Both coefficients, α and β , are greater for the radio channel case and the slope coefficient β is similar for the LoS case whereas it is higher for the OLoS case. Fig. 9 and Fig. 10 recall the normalized gain of the MPCs of the propagation channel and the radio channel from [7] and additionally show the model.

In order to use the fitted path gains in the hybrid channel model, the normalized path gains $G_{dB, \text{norm}, l}$ are unnormalized

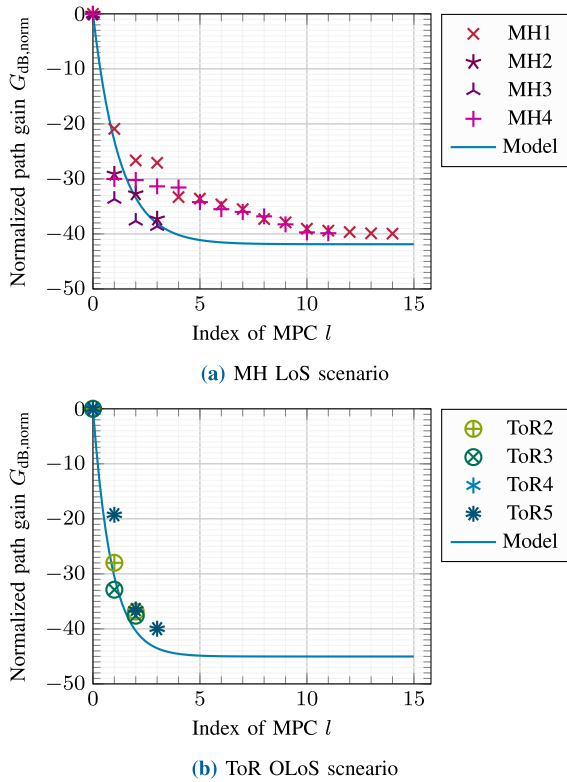


FIGURE 10. MPCs and approximation of the double-directional radio channel.

with respect to the strongest path of the ray-optical channel prediction. Then, the unnormalized gains are assigned to the respective MPCs from the ray-tracing with the same MPC index. This way, the gain with MPC index 1 replaces the second strongest gain from the ray-tracing, the third strongest replaces the third strongest etc. Conclusively, the resulting MPCs of the hybrid model get their geometric information from the deterministic channel prediction and their path gain from the analytic, empirical fit.

To evaluate the deviation of the analytic, empirical fit from the individually measured path gain of the MPCs, the error

$$E_{G,\text{dB},l} = 10 \log_{10} \left(\frac{1}{I} \sum_{i=1}^I 10^{\frac{|G_{\text{dB,meas},i,l} - G_{\text{dB,model},l}|}{10}} \right) \quad (15)$$

is evaluated that linearly averages a relative error measure of the I measurement positions. Table 7 and Table 8 present the global error and the error as a function of the MPC index l for the propagation channel and the radio channel, respectively. Generally, the error decreases with increasing MPC index. For MPC index 1, the error is significantly higher in the majority of scenarios which might reflect the variety of propagation states and the impact of the individual MPC at THz frequencies within a complex scenario.

The model in its presented form is valid for 15 MPCs. With greater number of MPCs the error would increase since the measured MPCs continue decreasing whereas the exponential model function converges to a minimum possible path gain. To account for even a higher number of MPCs the

TABLE 7. Error $E_{G,\text{dB},l}$ of the propagation channel model coefficients.

MPC index l	MH LoS	ToR LoS	ToR OLoS
overall	4.24	1.80	2.93
0	0	0	0
1	9.74	7.16	6.83
2	5.82	3.72	6.08
3	4.21	2.91	1.10
4	5.32	0.94	2.20
5	2.70	0.94	2.10
6	3.82	1.96	2.51
7	3.22	0.03	2.04
8	2.89	0.64	2.04
9	2.31	0.14	1.88
10	2.64	0.41	1.91
11	3.21	0.01	2.06
12	3.14	0.01	2.25
13	3.10	0.12	2.63
14	3.10	0.40	2.77
15	3.20	0.92	2.75

TABLE 8. Error $E_{G,\text{dB},l}$ of the radio channel model coefficients.

MPC index l	MH LoS	ToR LoS	ToR OLoS
overall	4.52	0.73	2.49
0	0	0	0
1	7.40	0.43	10.50
2	4.29	1.85	3.75
3	6.93	2.05	2.10
4	6.58	2.92	0.46
5	5.87	1.06	0.14
6	5.24	0.55	0.03
7	4.83	0.31	0.01
8	4.05	0.20	0.01
9	3.47	0.15	0.02
10	2.82	0.13	0.02
11	2.71	0.12	0.02
12	2.92	0.11	0.02
13	2.87	0.11	0.02
14	2.86	0.11	0.02
15	3.13	0.11	0.02

model function needs to be customized. Apart from that, the model might be adapted to a statistical approach defining probability density functions for the gain distribution for each MPC index. However, it is recommended to preserve the presented classification in order to account for the nature of propagation in the different scenarios.

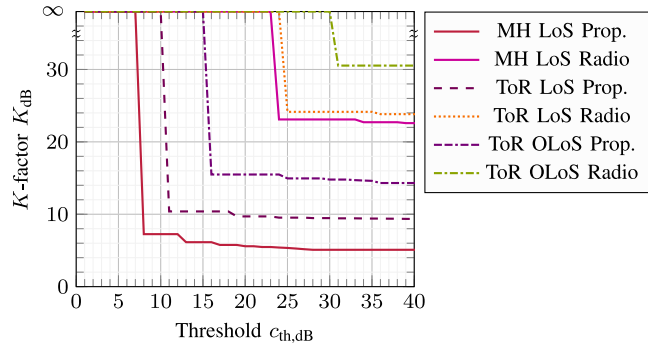
B. VERIFICATION OF THE CHANNEL MODEL

1) METHODOLOGY

The presented channel model for wireless links in a data center at THz frequencies is validated and checked for plausibility in the following section. It is reviewed if the most important MPCs are found and correctly represented such that the channel parameters and characteristics are useful for the development and design of novel THz communication systems. Therefore, six reference setups are simulated and the channel parameters are evaluated and compared in the same manner as presented in [7]. Since all double-directional measurements from [25] are used to determine the coefficients for the model of the channel gain in the respective categories, six separate setups are selected that are recapitulated in Table 9. MH LoS 5 m and MH LoS 10 m are comparable to MH2 and MH1, respectively. The other four setups are part of the P2P radio channel measurements in [25].

TABLE 9. Overview of TX and RX location for channel model validation.

ID	Scen.	r_{TX}/m	r_{RX}/m	d/m
MH LoS 5 m	LoS	(13.00 0.92 1.50)	(14.50 5.50 1.50)	4.81
MH LoS 10 m	LoS	(13.00 0.92 1.50)	(14.00 10.71 1.50)	9.84
P2P ToR DL3	LoS	(12.20 4.53 2.10)	(12.20 1.60 2.10)	2.926
P2P ToR DL5	LoS	(12.20 11.43 2.07)	(12.20 1.60 2.10)	9.828
P2P ToR DL6	OLoS	(14.96 3.12 2.07)	(9.00 3.12 2.07)	5.962
P2P ToR DL7	OLoS	(18.58 1.75 2.55)	(7.72 1.86 2.55)	10.86

**FIGURE 11.** K -factor of the modeled channels.

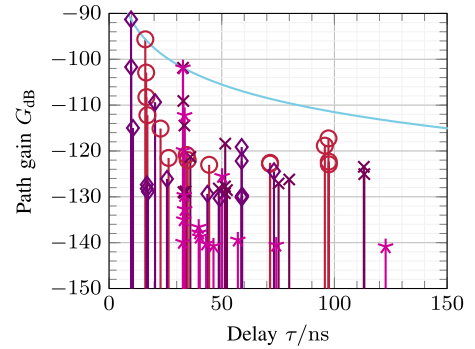
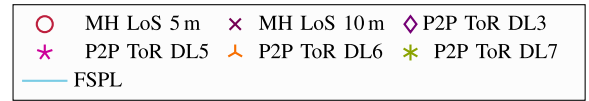
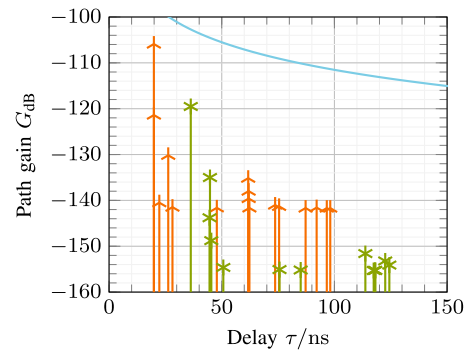
Designing a communication system involves specific requirements for system parameters, with the signal-to-noise ratio (SNR) being a critical metric. The prospective communication system only detects MPCs above the noise level, altering the channel characteristics based on the system's specifications. Unlike a universally constant channel parameter [51], the determination of relevant channel parameters for the specific communication system is influenced by a defined threshold $c_{th,dB}$, which sets the maximum allowable additional path loss with respect to the strongest MPC. Consequently, only MPCs exceeding this threshold are included in the channel parameter calculations. In the following, channel parameter definitions based on [7] are used.

2) COMPARISON OF CHANNEL PARAMETERS

The K -factor takes a special role since it refers only to the path gain ignoring any spatial or temporal characteristics. Hence, it is independent of the ray-optical channel prediction and identical for all realizations in the different model classes. Fig. 11 presents the K -factor for the six model classes as a function of the threshold $c_{th,dB}$.

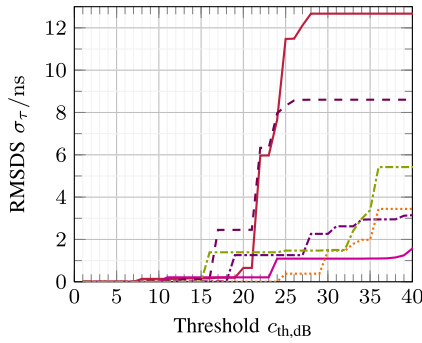
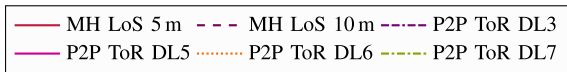
The K -factor shows the same behavior and similar values as the measured values in [7]. More specifically, the K -factor of ToR OLoS is higher than ToR LoS which is again higher than MH LoS. The values lie between 5 dB and 15 dB. This relation is repeated for the radio channel that obviously has higher K -factors with values between 22 dB and 32 dB.

To illustrate the shape of the created channel impulse response (CIR), their PDPs are visualized in Fig. 12 together with the free-space path loss (FSPL) that represents the theoretic limit of the path gain. The direct paths of the LoS scenarios agree with FSPL whereas the OLoS scenarios experience an additional attenuation of 8 dB and 16.7 dB. As a reminder, the measured values amount to 9.3 dB and 16.6 dB for P2P ToR DL6 and P2P ToR DL7, respectively. Hence, the

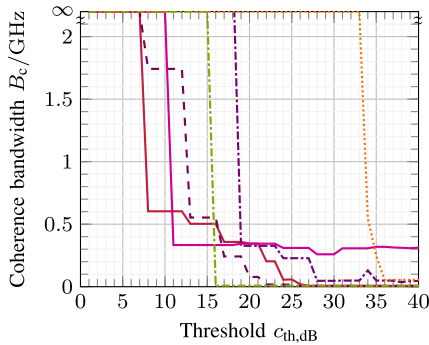
**(a)** LoS scenarios**(b)** OLoS scenarios**FIGURE 12.** PDPs of the modeled propagation channels.

path gain of the direct path that serves as reference for the denormalization is accurately predicted. Especially the MH LoS resemble well the measured PDPs in [7]. Thus, the visual impression of the model is convincing.

Also the channel parameters that depend on the path gain, the temporal and spatial characteristics form a compatible picture. The root mean square delay spread (RMSDS) presented in Fig. 13(a) shows a similar course in comparison with the RMSDS of the measured propagation channel. Starting at a threshold of 15 dB, the RMSDS increases for the MH scenarios that generally have a higher RMSDS than the ToR scenarios. At a threshold of 20 dB the RMSDSs in all scenarios increase with values between 1.8 ns to 6 ns for ToR scenarios and values between 8 ns and 13 ns for MH scenarios. The coherence bandwidth of the modeled CIRs is calculated according to [7] with a correlation level of 0.8 and plotted in Fig. 13(b). The drop of the coherence bandwidth occurs mainly in the interval of 8 dB to 20 dB that corresponds to the coherence bandwidth of the measured propagation channel. Also the late drop at a threshold greater than 30 dB for a ToR OLoS scenario is well represented. Once the coherence bandwidth is dropped, the modeled values lie partially above the measured ones with values between 0.2 GHz to 0.4 GHz compared to a coherence bandwidth below 0.2 GHz. This behavior might be due to the



(a) RMSDS



(b) Coherence bandwidth

FIGURE 13. RMSDS and coherence bandwidth of the modeled double-directional propagation channel.

limited number of MPCs but does not restrict the assertion or the applicability of the model since the nature of the channel is well represented.

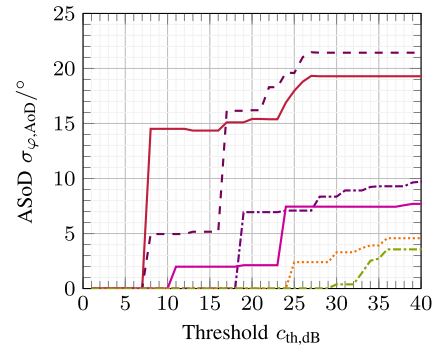
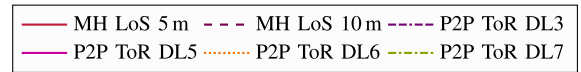
Finally, the angular spread (AS) that includes both, the path gain and the spatial characteristics, matches well with the measured characteristics of the propagation channel. Fig. 14 shows similar characteristics compared to the reference of the measured double-directional propagation channel in [7]. The maximum of the angular spread of departure (ASoD) is located around 20° whereas the angular spread of arrival (ASoA) in Fig. 14(b) reaches values up to 57° . The values of MH links are generally greater than the AS of ToR links which also agrees with the measured reference.

In conclusion, the validation shows that the model represents well the characteristics of wireless THz links for the different setups and is a novel resource to predict wireless channels for novel THz applications within data centers.

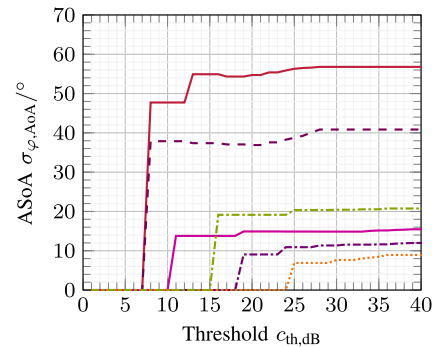
VI. CONCLUSION

The presented paper discusses relevant aspects for THz channel modeling with ray-optical channel predictions and presents a novel hybrid model approach that is applied to wireless links at THz frequencies in a data center.

In the context of ray-optical channel predictions that are appropriate by the nature of THz wave propagation,



(a) ASoD



(b) ASoA

FIGURE 14. ASs of the modeled double-directional propagation channel.

the necessary accuracy of a 3D model at THz frequencies ranging up to $100\mu\text{m}$ can hardly be achieved in complex environments. Also, the single interaction point of ray-tracing methodologies neglects the expansion of the incident beam on heterogeneous surfaces with holes.

Hence, a novel channel model approach combining deterministic ray-optical channel predictions and analytical, empirical models of the path gain is presented. Based on a detailed comparison of ray-optical channel predictions and measurements of the same scenarios, the benefits and accuracy of the prediction of spatial and temporal characteristics with ray-tracing are determined. The impact of scattering at THz frequencies contribute important MPCs and is not negligible. Scattering expresses itself in a specific cross-shaped figure for corridor-like environments that is observed in data centers, high-speed train wagons and aircraft cabins. However, due to the expected unsatisfactory predictions of path gain, an empirical, analytical model is established. The overall error for the individual MPCs in the data center is found to be below 5 dB.

Comparing resulting channel parameters of model realizations of the individual channel classes, the model is validated and proved to be suitable for the description of channels of wireless links in a data center at THz frequency. Also, the hybrid approach can be transferred to other scenarios representing a novel methodology of channel modeling in

complex scenarios. This way, the channel models contribute to realistic link level simulations of the physical layer and higher layer simulations of prospective THz communication systems.

ACKNOWLEDGMENT

The authors thank Mira Naftaly from the National Physics Laboratory (NPL), Teddington, U.K., for the material characterization.

REFERENCES

- [1] I. F. Akyildiz, C. Han, Z. Hu, S. Nie, and J. M. Jornet, "Terahertz band communication: An old problem revisited and research directions for the next decade," *IEEE Trans. Commun.*, vol. 70, no. 6, pp. 4250–4285, Jun. 2022, doi: [10.1109/TCOMM.2022.3171800](https://doi.org/10.1109/TCOMM.2022.3171800).
- [2] S. Rommel, T. R. Raddo, and I. T. Monroy, "Data Center connectivity by 6G wireless systems," in *Proc. Photon. Switch. Comput. (PSC)*. Limassol, Cyprus, 2018, pp. 1–3, doi: [10.1109/PS.2018.8751363](https://doi.org/10.1109/PS.2018.8751363).
- [3] A. S. Hamza, J. S. Deogun, and D. R. Alexander, "Wireless communication in data centers: A survey," *IEEE Commun. Surveys Tuts.*, vol. 18, no. 3, pp. 1572–1595, 3rd Quart., 2016, doi: [10.1109/COMST.2016.2521678](https://doi.org/10.1109/COMST.2016.2521678).
- [4] T. Benson, A. Akella, and D. A. Maltz, "Network traffic characteristics of data centers in the wild," in *Proc. 10th ACM SIGCOMM Conf. Internet Meas.*, Melbourne, VIC, Australia, 2010, pp. 267–280, doi: [10.1145/1879141.1879175](https://doi.org/10.1145/1879141.1879175).
- [5] W. Zhang, X. Zhou, L. Yang, Z. Zhang, B. Y. Zhao, and H. Zheng, "3D beamforming for wireless data centers," in *Proc. 10th ACM Workshop Hot Top. Netw.*, New York, NY, USA, 2011, pp. 1–6, doi: [10.1145/2070562.2070566](https://doi.org/10.1145/2070562.2070566).
- [6] S. Ahearne et al., "Integrating THz wireless communication links in a data centre network," in *Proc. IEEE 2nd 5G World Forum (5GWF)*, Dresden, Germany, 2019, pp. 393–398, doi: [10.1109/5GWF.2019.8911705](https://doi.org/10.1109/5GWF.2019.8911705).
- [7] J. M. Eckhardt, T. Doeker, and T. Kürner, "Channel measurements at 300 GHz for low Terahertz links in a data center," *IEEE Open J. Antennas Propag.*, vol. 5, pp. 759–777, 2024, doi: [10.1109/OJAP.2024.3391798](https://doi.org/10.1109/OJAP.2024.3391798).
- [8] J. M. Eckhardt and T. Doeker, "Lessons learned from a decade of THz channel sounding," *IEEE Commun. Mag.*, vol. 62, no. 2, pp. 24–30, Feb. 2024, doi: [10.1109/MCOM.001.2200586](https://doi.org/10.1109/MCOM.001.2200586).
- [9] C.-X. Wang, X. Cheng, and D. Laurenson, "Vehicle-to-vehicle channel modeling and measurements: Recent advances and future challenges," *IEEE Commun. Mag.*, vol. 47, no. 11, pp. 96–103, Nov. 2009, doi: [10.1109/MCOM.2009.5307472](https://doi.org/10.1109/MCOM.2009.5307472).
- [10] *Propagation Data and Prediction Methods for the Planning of Indoor Radiocommunication Systems and Radio Local Area Networks in the Frequency Range 300 MHz to 450 GHz*, Rec. ITU-R P.1238-12, International Telecommunications Union, Geneva, Switzerland, Aug. 2023. [Online]. Available: <https://www.itu.int/rec/R-REC-P.1238>
- [11] J. M. Eckhardt, V. Petrov, D. Moltchanov, Y. Koucheryavy, and T. Kürner, "Channel measurements and modeling for low-Terahertz band vehicular communications," *IEEE J. Select. Areas Commun.*, vol. 39, no. 6, pp. 1590–1603, Jun. 2021, doi: [10.1109/JSAC.2021.3071843](https://doi.org/10.1109/JSAC.2021.3071843).
- [12] T. Doeker, J. M. Eckhardt, and T. Kürner, "Channel measurements and modeling for low Terahertz communications in an aircraft cabin," *IEEE Trans. Antennas Propag.*, vol. 70, no. 11, pp. 10903–10916, Nov. 2022, doi: [10.1109/TAP.2022.3191218](https://doi.org/10.1109/TAP.2022.3191218).
- [13] H. Yi et al., "Ray tracing meets Terahertz: Challenges and opportunities," *IEEE Commun. Mag.*, vol. 62, no. 2, pp. 40–46, Feb. 2024, doi: [10.1109/MCOM.001.2200454](https://doi.org/10.1109/MCOM.001.2200454).
- [14] S. Priebe and T. Kürner, "Stochastic modeling of THz indoor radio channels," *IEEE Trans. Wireless Commun.*, vol. 12, no. 9, pp. 4445–4455, Sep. 2013, doi: [10.1109/TWC.2013.072313.121581](https://doi.org/10.1109/TWC.2013.072313.121581).
- [15] K. Guan, H. Yi, D. He, B. Ai, and Z. Zhong, "Towards 6G: Paradigm of realistic Terahertz channel modeling," *China Commun.*, vol. 18, no. 5, pp. 1–18, May 2021, doi: [10.23919/JCC.2021.05.001](https://doi.org/10.23919/JCC.2021.05.001).
- [16] C. Han et al., "Terahertz wireless channels: A holistic survey on measurement, modeling, and analysis," *IEEE Commun. Surveys Tuts.*, vol. 24, no. 3, pp. 1670–1707, 3rd Quart., 2022, doi: [10.1109/COMST.2022.3182539](https://doi.org/10.1109/COMST.2022.3182539).
- [17] S. Mollahasani and E. Onur, "Evaluation of Terahertz channel in data centers," in *Proc. Proc. IEEE/IFIP Netw. Oper. Manag. Symp. (NOMS)*, Istanbul, Turkey, 2016, pp. 727–730, doi: [10.1109/NOMS.2016.7502886](https://doi.org/10.1109/NOMS.2016.7502886).
- [18] B. Peng and T. Kürner, "A stochastic channel model for future wireless THz data Centers," in *Proc. Int. Symp. Wireless Commun. Syst. (ISWCS)*, Brussels, Belgium, 2015, pp. 741–745, doi: [10.1109/ISWCS.2015.7454448](https://doi.org/10.1109/ISWCS.2015.7454448).
- [19] A. Fricke, "TG3d Channel Modeling Document (CMD), IEEE P802.15 Working Group for Wireless Personal Area Networks (WPANs)," Inst. Elect. Electron. Eng., Piscataway, NJ, USA, document 15-14-0310-19-003d, Mar. 2016. [Online]. Available: <https://mentor.ieee.org/802.15/dcn/14/15-14-0310-19-003d-channel-modeling-document.docx>
- [20] C.-L. Cheng, S. Sangodoyin, and A. Zajic, "THz MIMO channel characterization for wireless data center-like environment," in *Proc. IEEE Int. Symp. Antennas Propag. (ISAP) (USNC-URSI Radio Sci. Meet.)*, Atlanta, GA, USA, 2019, pp. 2145–2146, doi: [10.1109/APUSNCURSINRSM.2019.8889030](https://doi.org/10.1109/APUSNCURSINRSM.2019.8889030).
- [21] C.-L. Cheng, S. Sangodoyin, and A. Zajic, "Terahertz MIMO fading analysis and doppler modeling in a data Center environment," in *Proc. 14th Eur. Conf. Antennas Propag. (EuCAP)*, Copenhagen, Denmark, 2020, pp. 1–5, doi: [10.23919/EuCAP48036.2020.9135695](https://doi.org/10.23919/EuCAP48036.2020.9135695).
- [22] C.-L. Cheng, S. Sangodoyin, and A. Zajic, "THz cluster-based modeling and propagation characterization in a data center environment," *IEEE Access*, vol. 8, pp. 56544–56558, 2020, doi: [10.1109/ACCESS.2020.2981293](https://doi.org/10.1109/ACCESS.2020.2981293).
- [23] G. Song et al., "Channel measurement and characterization at 140 GHz in a wireless data center," in *Proc. IEEE Glob. Commun. Conf. (GLOBECOM)*, Rio de Janeiro, Brazil, 2022, pp. 4764–4769, doi: [10.1109/GLOBECOM48099.2022.10001052](https://doi.org/10.1109/GLOBECOM48099.2022.10001052).
- [24] *Propagation Data and Prediction Methods for the Planning of Indoor Radiocommunication Systems and Radio Local Area Networks in the Frequency Range 300 MHz to 450 GHz*, Rec. ITU-R P.1238-11, International Telecommunications Union, Geneva, Switzerland, Sep. 2021. [Online]. Available: <https://www.itu.int/rec/R-REC-P.1238>
- [25] J. M. Eckhardt, T. Doeker, and T. Kürner, *Calibrated Impulse Responses and Extracted Multipath Components from Channel Sounding at 300 GHz in a Data Center*, Technische Universität Braunschweig, Braunschweig, Germany, 2023, doi: [10.24355/dbbs.084-202312041057-0](https://doi.org/10.24355/dbbs.084-202312041057-0).
- [26] R. Piesiewicz, *Propagation Aspects and Performance Study of Future Indoor Wireless Communication Systems at THz Frequencies*. Aachen, Germany: Shaker Verlag, 2009.
- [27] F. Taleb, G. G. Hernandez-Cardoso, E. Castro-Camus, and M. Koch, "Transmission, reflection and scattering characterization of building materials for indoor THz communications," *IEEE Trans. THz Sci. Technol.*, vol. 13, no. 5, pp. 421–430, Sep. 2023, doi: [10.1109/TTHZ.2023.3281773](https://doi.org/10.1109/TTHZ.2023.3281773).
- [28] F. Taleb, "Optical parameters and scattering coefficient," Dataset, Figshare, London, U.K., Nov. 2022, doi: [10.6084/m9.figshare.21539109.v3](https://doi.org/10.6084/m9.figshare.21539109.v3).
- [29] S. Sahin, N. K. Nahar, and K. Sertel, "Dielectric properties of low-loss polymers for mmW and THz applications," *J. Infrared Millim. Terahertz Waves*, vol. 40, no. 5, pp. 557–573, May 2019, doi: [10.1007/s10762-019-00584-2](https://doi.org/10.1007/s10762-019-00584-2).
- [30] Y.-S. Jin, G.-J. Kim, and S.-G. Jeon, "Terahertz dielectric properties of polymers," *J. Korean Phys. Soc.*, vol. 49, no. 2, pp. 513–517, Aug. 2006, doi: [10.1109/IRMMW-THz50926.2021.9567129](https://doi.org/10.1109/IRMMW-THz50926.2021.9567129).
- [31] A. Prokscha, F. Sheikh, M. Al-Hasan, I. Mabrouk, and T. Kaiser, "Blockage impact of human locomotion gaits on Terahertz wireless links," in *Proc. 46th Int. Conf. Infrared Millim. Terahertz Waves (IRMMW-THz)*, Chengdu, China, 2021, pp. 1–2, doi: [10.1109/IRMMW-THz50926.2021.9567129](https://doi.org/10.1109/IRMMW-THz50926.2021.9567129).
- [32] J.-M. Lourtioz, *Photonic Crystals: Towards Nanoscale Photonic Devices*. Berlin, Germany: Springer, 2005.
- [33] *Propagation Data and Prediction Methods for the Planning of Indoor Radiocommunication Systems and Radio Local Area Networks in the Frequency Range 900 MHz to 100 GHz*, Recommendation ITU-R P.1238-7, International Telecommunications Union, Geneva, Switzerland, Feb. 2012. [Online]. Available: <https://www.itu.int/rec/R-REC-P.1238>

- [34] J. M. Eckhardt, B. K. Jung, T. Doeker, M. Naftaly, and T. Kürner, "Terahertz based ultra high bandwidth wireless access networks, D4.4 final characterization of systems," Terapod, Brussels, Belgium, Rep. D4.4, Jun. 2020, doi: [10.3030/761579](https://doi.org/10.3030/761579).
- [35] J. M. Eckhardt, *THz Communications in a Data Center: Channel Measurements, Modeling and Physical Layer Analysis* (Mitteilungen Aus Dem Institut Für Nachrichtentechnik). Düren, Germany: Shaker Verlag, Jun. 2024, doi: [10.24355/dbbs.084-202405061045-0](https://doi.org/10.24355/dbbs.084-202405061045-0).
- [36] L. F. Chen, C. K. Ong, C. P. Neo, V. V. Varadan, and V. K. Varadan, *Microwave Electronics: Measurement and Materials Characterization*, 1st ed. Hoboken, NJ, USA: Wiley, Mar. 2004, doi: [10.1002/0470020466](https://doi.org/10.1002/0470020466).
- [37] M. Born and E. Wolf, *Principles of Optics: 60th Anniversary Edition*, 7th ed. Cambridge, U.K.: Cambridge Univ. Press, Dec. 2019, doi: [10.1017/9781108769914](https://doi.org/10.1017/9781108769914).
- [38] *Simulator for Mobile Networks*, Technische Universität Braunschweig, Braunschweig Germany, 2023. [Online]. Available: <https://www.tu-braunschweig.de/en/ifn/research/simone>
- [39] M. Schweins, L. Thielecke, N. Grupe, and T. Kürner, "Optimization and evaluation of a 3D ray tracing channel predictor individually for each propagation effect," *IEEE Open J. Antennas Propag.*, vol. 5, pp. 495–506, 2024, doi: [10.1109/OJAP.2024.3366070](https://doi.org/10.1109/OJAP.2024.3366070).
- [40] J. M. Eckhardt, C. Herold, B. K. Jung, N. Dreyer, and T. Kürner, "Modular link level simulator for the physical layer of beyond 5G wireless communication systems," *Radio Sci.*, vol. 57, no. 2, pp. 1–5, Feb. 2022, doi: [10.1029/2021RS007395](https://doi.org/10.1029/2021RS007395).
- [41] D. M. Rose, J. Baumgarten, S. Hahn, and T. Kürner, "SiMoNe-simulator for mobile networks: System-level simulations in the context of realistic scenarios," in *Proc. IEEE 81st Veh. Technol. Conf. (VTC Spring)*. Glasgow, U.K., 2015, pp. 1–7, doi: [10.1109/VTCSpring.2015.7146084](https://doi.org/10.1109/VTCSpring.2015.7146084).
- [42] N. Dreyer and T. Kürner, "An analytical raytracer for efficient D2D path loss predictions," in *Proc. 13th Eur. Conf. Antennas Propag. (EuCAP)*, Krakow, Poland, 2019, pp. 1–5. [Online]. Available: <https://ieeexplore.ieee.org/document/8739409>
- [43] J. G. Meana, J. Á. Martínez-Lorenzo, F. Las-Heras, and C. Rappaport, "Wave scattering by dielectric and lossy materials using the modified equivalent current approximation (MECA)," *IEEE Trans. Antennas Propag.*, vol. 58, no. 11, pp. 3757–3761, Nov. 2010, doi: [10.1109/TAP.2010.2071363](https://doi.org/10.1109/TAP.2010.2071363).
- [44] C. Jansen et al., "Diffuse scattering from rough surfaces in THz communication channels," *IEEE Trans. Terahertz Sci. Technol.*, vol. 1, no. 2, pp. 462–472, Nov. 2011, doi: [10.1109/TTHZ.2011.2153610](https://doi.org/10.1109/TTHZ.2011.2153610).
- [45] R. Piesiewicz, C. Jansen, D. Mittleman, T. Kleine-Ostmann, M. Koch, and T. Kürner, "Scattering analysis for the modeling of THz communication systems," *IEEE Trans. Antennas Propag.*, vol. 55, no. 11, pp. 3002–3009, Nov. 2007, doi: [10.1109/TAP.2007.908559](https://doi.org/10.1109/TAP.2007.908559).
- [46] K. Guan et al., "Channel Characterization for intra-wagon communication at 60 and 300 GHz bands," *IEEE Trans. Veh. Technol.*, vol. 68, no. 6, pp. 5193–5207, Jun. 2019, doi: [10.1109/TVT.2019.2907606](https://doi.org/10.1109/TVT.2019.2907606).
- [47] S. Priebe, *Towards THz Communications: Propagation Studies, Indoor Channel Modeling and Interference Investigations*. Aachen, Germany: Shaker Verlag, 2013.
- [48] M. Jacob, S. Priebe, R. Dickhoff, T. Kleine-Ostmann, T. Schrader, and T. Kürner, "Diffraction in Mm and sub-Mm wave indoor propagation channels," *IEEE Trans. Microw. Theory Techn.*, vol. 60, no. 3, pp. 833–844, Mar. 2012, doi: [10.1109/TMTT.2011.2178859](https://doi.org/10.1109/TMTT.2011.2178859).
- [49] K. Guan et al., "Channel sounding and ray tracing for intrawagon scenario at mmWave and sub-mmWave bands," *IEEE Trans. Antennas Propag.*, vol. 69, no. 2, pp. 1007–1019, Feb. 2021, doi: [10.1109/TAP.2020.3016399](https://doi.org/10.1109/TAP.2020.3016399).
- [50] J. M. Eckhardt et al., "Uniform analysis of multipath components from various scenarios with time-domain channel sounding at 300 GHz," *IEEE Open J. Antennas Propag.*, vol. 4, pp. 446–460, 2023, doi: [10.1109/OJAP.2023.3263597](https://doi.org/10.1109/OJAP.2023.3263597).
- [51] R. Schulpen, U. Johannsen, A. B. Smolders, and L. A. Bronckers, "Ambiguity in RMS delay spread of millimeter-wave channel measurements," in *Proc. 17th Eur. Conf. Antennas Propag. (EuCAP)*, Florence, Italy, 2023, pp. 1–5, doi: [10.23919/EuCAP57121.2023.10133511](https://doi.org/10.23919/EuCAP57121.2023.10133511).



JOHANNES M. ECKHARDT (Member, IEEE) received the Dipl.-Ing. degree in electrical engineering from Technische Universität Dresden, Germany, in 2017, the M.A. degree from Ecole Centrale Paris, France, in 2017, and the Dr.-Ing. degree from Technische Universität Braunschweig, Germany, in 2024, where he is currently a Research Associate with the Department of Mobile Radio Systems, Institute for Communications Technology. His research interests include channel measurements and modeling, link-level simulations and interference studies in complex scenarios for multi gigabit communication systems at THz frequencies. In 2023, he was awarded the "VDE ITG Preis" for an outstanding publication.



TOBIAS DOEKER (Graduate Student Member, IEEE) received the B.Sc. degree from the Hamburg University of Applied Science in 2017 and the M.Sc. degree in electrical engineering with a focus on communications technology from Technische Universität Braunschweig in 2019, where he is currently pursuing the Ph.D. degree. Besides, he was a Student Trainee at Lufthansa Technik AG, Hamburg, from 2013 to 2019. In November 2019, he joined as a Researcher with the Institute for Communications Technology, Technische Universität Braunschweig. His research interests include THz communications, radio channel measurements, and characterization as well as device discovery for multi gigabit indoor communication at 300 GHz. In 2023, he received the "VDE ITG Preis" for an outstanding publication in the IEEE TRANSACTIONS ON ANTENNAS AND PROPAGATION.



THOMAS KÜRNER (Fellow, IEEE) received the Dipl.-Ing. degree in electrical engineering and the Dr.-Ing. degree from the University of Karlsruhe, Germany, in 1990 and 1993, respectively, where he was with the Institut für Höchstfrequenztechnik und Elektronik working on wave propagation modeling, radio channel characterization, and radio network planning from 1990 to 1994. From 1994 to 2003, he was with the Radio Network Planning Department, Headquarters of the GSM 1800 and UMTS operator E-Plus Mobilfunk GmbH & Co KG, Düsseldorf, where he was team manager radio network planning support. Since 2003, he has been a Full University Professor for Mobile Radio Systems with the Technische Universität Braunschweig. In 2012, he was a Guest Lecturer with Dublin City University within the Telecommunications Graduate Initiative, Ireland. He is currently the chairing the IEEE 802.15 Standing Committee THz and the ETSI Industrial Specification Group THz. He was also the Chair of IEEE 802.15.3d TG 100G, which developed the worldwide first wireless communications standard operating at 300 GHz. He was the Project Coordinator of the H2020-EU-Japan project ThoR ("TeraHertz end-to-end wireless systems supporting ultra-high data Rate applications") and is Coordinator of the German DFG-Research Unit FOR 2863 Meteracom ("Metrology for THz Communications"). In 2019 and 2022, he was the recipient of the Neal-Shephard Award of the IEEE Vehicular Technology Society. From 2016 to 2021, he was a member of the Board of Directors of the European Association on Antennas and Propagation and from 2020 to 2022, and a Distinguished Lecturer of IEEE VEHICULAR TECHNOLOGY SOCIETY.